

Article

Polypyrrole Modified Carbon Nanotube/Polyimide Electrode Materials for Supercapacitors and Lithium-ion Batteries

Ruchinda Gooneratne and Jude O. Iroh * 

Department of Mechanical and Materials Engineering, University of Cincinnati, Cincinnati, OH 45221, USA

* Correspondence: irohj@ucmail.uc.edu

Abstract: Lithium-ion batteries have evolved and transcended in recent years to power every device across the spectrum, from watches to electrical vehicles and beyond. However, the lithium-ion battery requires the use of heavy and expensive transition metal oxides that have limited life cycles. Conductive polymer nanocomposites have been shown to possess good electrochemical and thermomechanical properties and are considered to be effective alternatives to transition metal oxides. The fabrication and properties of polyimide matrix-single wall carbon nanotube, SWCNT composite electrode materials, modified by the electrodeposition of polypyrrole, PPy was successfully carried out. The doping of PPy with p-Toluene sulfonic acid, T resulted in a dramatic transformation of the morphology and specific capacitance of the electrode material. Electrochemical impedance spectroscopy, EIS, cyclic voltammetry, CV, and galvanic charge–discharge tests were used to measure the electrode’s specific capacitance and specific capacity. Maximum specific capacitance values of up to 84.88 F/g and 127.13 F/g were obtained by CV and charge–discharge tests, respectively. A capacitance retention of over 80% was obtained after over 500 cycles of testing. The insertion of doped PPy into the electrode material by electrochemical polymerization was shown to positively correlate to the improved electrochemical performance of the nanocomposite. An increase in the porosity of about 34.68% over the non-doped polypyrrole was obtained from EIS measurement and supported by the optical microscope pictures. Increasing the process parameters, such as pyrrole, Py concentration and the amount of dopants, lead to a dramatic increase in the specific capacitance and capacity of the composite electrodes.

Keywords: polypyrrole; p-Toluene sulfonic acid; polyimide carbon nanotube composite; electrochemical; supercapacitor; conducting polymer



Citation: Gooneratne, R.; Iroh, J.O. Polypyrrole Modified Carbon Nanotube/Polyimide Electrode Materials for Supercapacitors and Lithium-ion Batteries. *Energies* **2022**, *15*, 9509. <https://doi.org/10.3390/en15249509>

Academic Editor: Carlos Miguel Costa

Received: 30 October 2022
Accepted: 10 December 2022
Published: 15 December 2022

Publisher’s Note: MDPI stays neutral with regard to jurisdictional claims in published maps and institutional affiliations.



Copyright: © 2022 by the authors. Licensee MDPI, Basel, Switzerland. This article is an open access article distributed under the terms and conditions of the Creative Commons Attribution (CC BY) license (<https://creativecommons.org/licenses/by/4.0/>).

1. Introduction

Conducting polymers (CPs) are widely used in energy storage applications in supercapacitors and batteries. Supercapacitors are energy storage devices that store electrical energy between the electric double layer. They possess very high-power densities, charge cyclabilities, and service lifespans [1–4]. Supercapacitors are capable of storing and releasing stored energy instantaneously. Our world is rapidly advancing, such that we have become dependent on energy storage devices. The demand for these devices to be lighter, safer, and higher-performing grows stronger every day. CP’s excellent electrical properties, high surface porosity, and compatibility with polymers and activated carbon composites make them a valuable resource for supercapacitors [4–6]. Many approaches to synthesizing CPs are well known, including pyrolysis, and photochemical, chemical, and electrochemical polymerization. The preferred technique for the synthesis of PPy is determined by the desired application [7–10]. Electrochemical synthesis, however, is the most effective synthetic technique for energy storage applications, due to its ability to produce doped PPy thin uniform films on conductive substrates. It is also cost-effective, allowing for reduced material usage (oxidizers) and relatively high purity of the feed materials [11].

Polypyrrole (PPy) is an intrinsically conducting polymer capable of storing energy by forming an electric double layer [12]. In addition to the electric double layer storage mechanism of PPy and other conducting polymers, PPy can store electric charge by undergoing a redox reaction, resulting in a pseudocapacitive behavior [13,14]. The presence of conjugated double bonds in their structure makes them electroactive in both aqueous and organic mediums. PPy's electrical conductivity ranges from 10^{-4} to 10^{-2} S/cm [10,11,15,16]. Studies have shown that PPy's electrical and electrochemical properties can be enhanced by doping. Doping can be performed by using inorganic and organic acids as well as polymeric stabilizers which tune the morphology of PPy, and, in turn, affect its electrochemical properties [14]. Dodecylbenzene sulfonic acid- and camphor sulfonic acid-doped PPy have shown increased conductivities of about 5 S/cm and 18 S/cm, respectively [17,18]. Lü successfully synthesized p-Toluene sulfonic acid-doped PPy nanoparticles with an electrical conductivity of about 52.7 S/cm [19,20].

The processability, mechanical properties, and stability of neat PPy are relatively low because of inherent structural damage after prolonged cycling [14,20]. However, the properties of PPy can be significantly enhanced by combining PPy with activated carbons or other polymers to create composite structures with an improved electrochemical performance [9,13,20]. Carbon nanotubes (CNTs) are exceptional conductive nanofiller materials with very high mechanical properties and specific surface areas [4,14]. They are often used in the fabrication of supercapacitor electrodes in combination with hybrid Germanium-carbon electrodes, which have a specific capacity of about 800 mAh/g [21,22].

Polyimides (PI) have also been shown to be excellent polymer matrices that permit the homogenous dispersion and formation of polymeric CNT nanocomposites [23]. Polyimides are high-performance polymers with excellent mechanical and thermal properties. Polyimide composites have a wide range of useful applications [24–27]. Huang et al. prepared an asymmetric MnO_2/CNT and PI/CNT supercapacitors, and reported a specific capacitance of 32.8 Fg^{-1} at 0.74 mAcm^{-2} in a carboxymethyl cellulose sodium sulfate electrolyte [28].

In this paper, we report the effect of the electrodeposition of p-Toluene sulfonic acid (pTSA)-doped polypyrrole onto composite single-walled carbon nanotube/polyimide electrodes. The insertion of the dopant into the PPy structure during electrochemical polymerization had a remarkable impact on the electrode's electrochemical properties, including the specific gravimetric capacitance, bulk resistance, and capacitance retention.

2. Materials and Methods

2.1. Materials

The materials used in this study include reagent-grade (ACS) N,N-Dimethylformamide (DMF) purchased from Right Price Chemicals. Pyromellitic dianhydride (PMDA) 99% purity, 4,4-oxydianiline (ODA), and pyrrole monomer (reagent grade 98% purity) were purchased from Sigma-Aldrich. The dopant for this experiment, p-Toluene sulfonic acid, was also purchased from Sigma-Aldrich. The single-walled carbon nanotubes (SWCNTs) were obtained from TuballTM, Leudelange, Luxembourg. All chemicals were used as received.

2.2. In-Situ Synthesis of Polyimide/SWCNT

A batch of SWCNTs determined to be 50 wt% was dispersed in DMF under both sonication and mechanical stirring (320RPM) for 3 h. The suspension was maintained at a constant temperature of 5°C using a constant temperature water bath. ODA (0.0245 mol) was then added to the suspension and sonicated under continuous stirring for an additional 1 h. The solution was then transferred to a 3-neck flask where a constant stream of pure nitrogen gas (50 mL/min) was introduced for the duration of the synthesis. PMDA (0.0245 mol) was carefully added into this solution and stirred at 220 RPM, allowing it to polymerize for 90 min at 5°C . An observable increase in the solution's viscosity was noticed during the synthesis, with the solution thickening to a honey-like consistency.

The polymer nanocomposite films were cast (0.5 mm wet thickness) onto a Teflon sheet using an MTI vacuum-assisted film coater. Initial curing was carried out at 80 °C for 1 h until any visible solvent had dried out. The film was then transferred into a vacuum oven where it was cured stepwise at 120 °C for 4 h, 180 °C for 3 h, 200 °C for 1 h, and then 250 °C for another 1 h under a vacuum of 28 in.Hg throughout the entire curing process. The cured film was peeled off the Teflon sheet after it had cooled down and was cut into rectangular electrodes for electrochemical deposition of PPy, and/or characterization.

2.3. Polypyrrole Electrodeposition and Doping

Pyrrole, Py was dissolved in 100 mL of water to make samples of 0.05 M, 0.1 M, and 0.5 M concentrations. Each batch of pyrrole was mixed with 0.0225 M, 0.1 M, and 0.2 M p-Toluene sulfonic acid by mechanical stirring until complete dissolution and a clear solution was obtained. The SWCNT/PI (films) working electrodes were immersed in each solution in a three-electrode cell configuration connected to a Gamry 3000 potentiostat. A glassy carbon counter electrode and Ag/AgCl reference electrode were used in electrochemical polymerization. Potentiostatic electrochemical polymerization was carried out for 600 s at 2 V. After the deposition of polypyrrole was completed, each electrode was carefully washed with ethanol, dried in a vacuum oven at 100 °C to remove any moisture, and weighed. Electrochemical characterization was carried out on the electrodes to measure the gravimetric capacitance, bulk resistivity, and capacitance retention after multiple charge–discharge cycles. The electrochemical properties were measured by using the Gamry 3000 Potentiostat operated in cyclic voltammetry, electrochemical impedance spectroscopy, and cyclic charge–discharge modes, respectively. A solution of 1M H₂SO₄ was used as the electrolyte.

3. Characterization

3.1. Scanning Electron Microscopy (SEM)

A Thermo Fisher SCIOS DualBeam SEM was utilized to observe the surface morphology of the electrodes at both 1000× and 10,000× magnification. Gold sputtering was not necessary as samples were already conductive.

3.2. Cyclic Voltammetry

Electrochemical characterization was carried out using the Gamry 3000 potentiostat in a 3-electrode cell configuration with an Ag/AgCl reference electrode. Cyclic voltammetry (CV) was done in a voltage range between 0 V to 1 V at three different scan rates of 5, 10, and 25 mV/s to determine the specific gravimetric capacitance (C_p) of the electrode material before and after deposition of PPy with different dopants. Equation (1a) was used to calculate the C_p in F/g, where I (A) is the response current obtained during the voltage sweep ΔV (V) at given scan rates v (mV/s) of the specific active material m (g). $\int IdV$ is the integrated area under the cyclic voltammetry curve [13].

$$C_p = \frac{\int IdV}{2m \times v \times \Delta V} \quad (1a)$$

Specific capacity of the material (C_{sp}) in mAh/g was calculated using Equation (1b).

$$C_{sp} = \frac{\int IdV}{2m \times v \times 3.6} \quad (1b)$$

Capacitance retention was calculated by dividing successive discharge capacitance by the discharge capacitance of the 2nd cycle.

3.3. Gravimetric Cyclic Charge/Discharge

Samples were cycled under galvanostatic conditions at three different current densities: 0.5 A/g, 1 A/g, and 5 A/g from 0 V to 0.8 V. The many cycles of test on the sample also

provided information on the material's charge retention properties. Specific capacitance (C_p) F/g was calculated using Equation (2), where I_m is the discharge current density (Ag^{-1}), Δt is the discharge time (s), and ΔV is the drop in voltage (V) during that discharge period [29].

$$C_p = \frac{I_m \Delta t}{\Delta V} \quad (2)$$

3.4. Electrochemical Impedance Spectroscopy (EIS)

EIS measurements were done in a frequency range from 1 MHz to 0.01 Hz and the results were modeled against a Randle's cell equivalent electrical circuit with a Warburg element, shown in Figure 1.

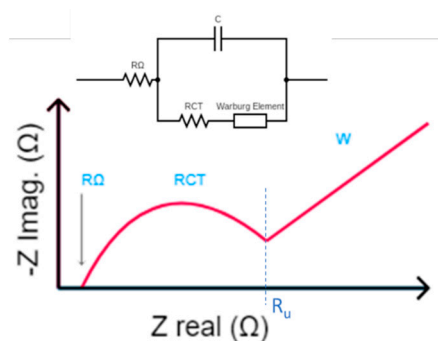


Figure 1. Equivalent Randle's cell circuit model with Warburg element for EIS Nyquist plot fitting.

A modified form of Archie's law, Equations (3a) and (3b), were used to estimate the electrode porosity from EIS data [30,31]:

$$\sigma_{eff} = \frac{t}{R_u A} \quad (3a)$$

$$\varnothing = \sqrt[m]{\frac{\sigma_{eff}}{\sigma_0 C}} \quad (3b)$$

where σ_{eff} is the effective electrical conductivity of the electrode, t and A are the thickness and contact area of the active electrode, respectively, R_u is the bulk resistance, C is the coefficient of saturation ranging from 0.1 to 1, σ_0 is the electrolyte conductivity, m is the cementation factor (typically between 1.5 to 4), and \varnothing is the sample's porosity [30,31].

EIS models for calculating specific capacitance (C_p) are based on the Bode and Nyquist plots using Equation (4), where f is the corresponding Bode frequency (s^{-1}) at the max imaginary impedance (Z''), which is the peak of the Nyquist semicircle plot, Z'_{max} is the corresponding real impedance (Ω), and m is the mass of bulk electrode material in contact with electrolyte (g):

$$C_p = \frac{1}{2\pi f Z'_{max} \times m} \quad (4)$$

3.5. Fourier Transform Infrared Spectroscopy—FTIR

A Nicolet 6700 FT-IR spectroscope equipped with a germanium crystal ATR was used to analyze the chemical composition of the samples before and after the doped PPy was deposited. Samples were scanned 32 times between the wavenumber ranges of 4000 cm^{-1} and 650 cm^{-1} .

4. Results and Discussion

4.1. Scanning Electron Microscopy

Figures 2 and 3 show a much clearer effect/change in the surface morphology at different dopant and Py concentrations. Increasing the dopant concentration from 0.0225 TSA to 0.1 TSA for 0.5M Py resulted in more pronounced surface features appearing on the elec-

trode. Compared to having kept the dopant concentrations constant, increasing Py did not seem to show as much of a prominent development of 3D-like surface depositions/globules.

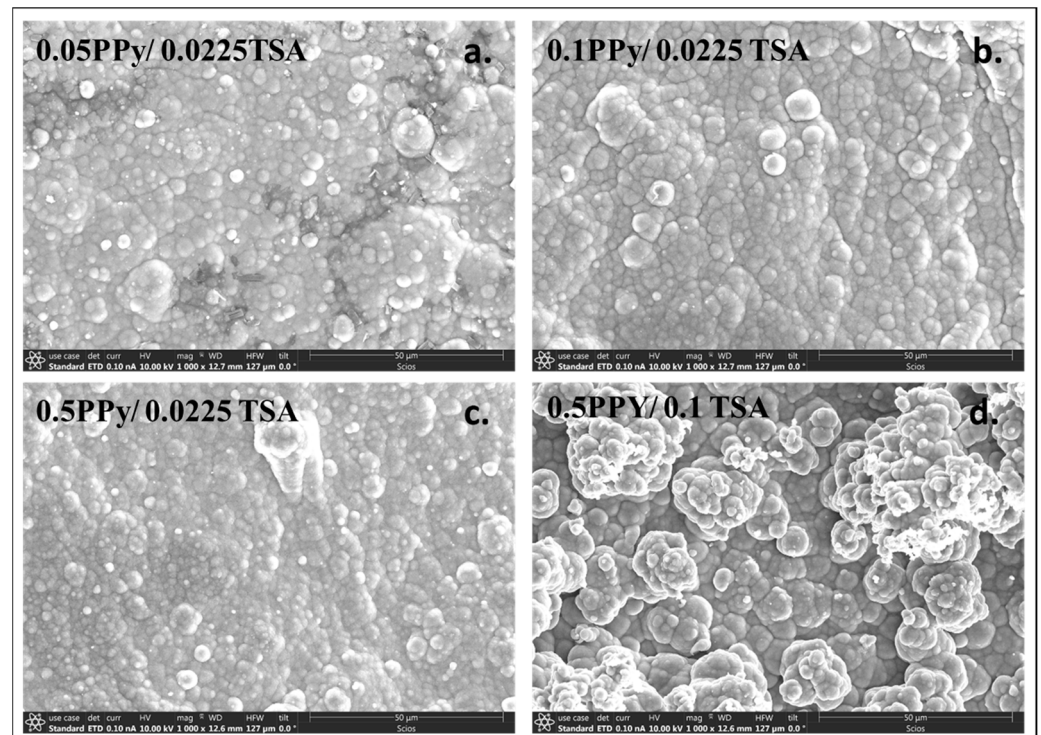


Figure 2. 1000× magnification showing the effect of dopant and Py concentration on PPy deposition and resulting surface morphology.

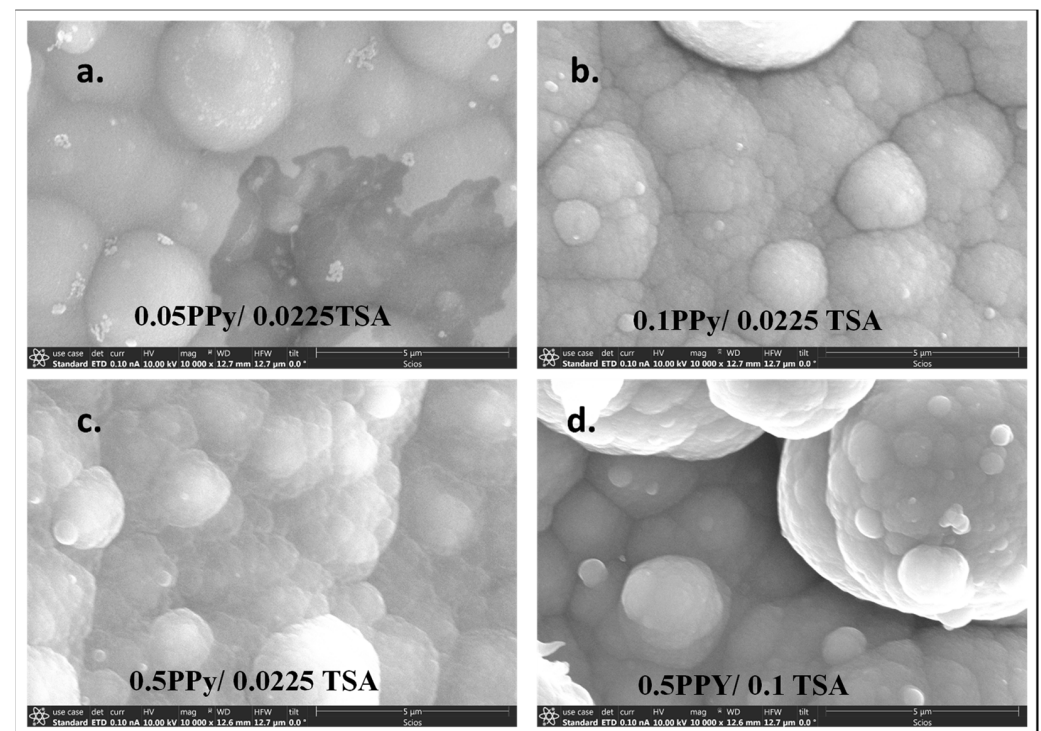


Figure 3. 10,000× magnification showing the effect of dopant and Py concentration on PPy deposition and resulting surface morphology.

4.2. Cyclic Voltammetry

Figure 4a shows the cyclic voltammograms of the 50 wt% SWCNT/PI nanocomposite electrodes tested in the 1M H₂SO₄ electrolyte solution at the varied Py and p-Toluene sulfonic acid concentrations. Scan rates of 5, 10, and 25 mV/s were each used to run the CV tests. The results from the CV tests were used to estimate the charge storage capabilities of the electrodes and determine how they were affected by the dopant concentration. All of the electrodes showed good cycling stability between 0 V to 1 V with high response currents of up to 30 mA. The addition of PPy improved the voltammograms by increasing the amount of charge stored in the electrode material as indicated by a larger integrated area under the curve. The square-shaped voltammograms with the absence of visible redox peaks are indicative of the supercapacitor behavior of the electrode material even at low scan rates. The increase in response currents at higher scan rates in Figure 4b is suggestive of good capacitive properties of the electrode [32].

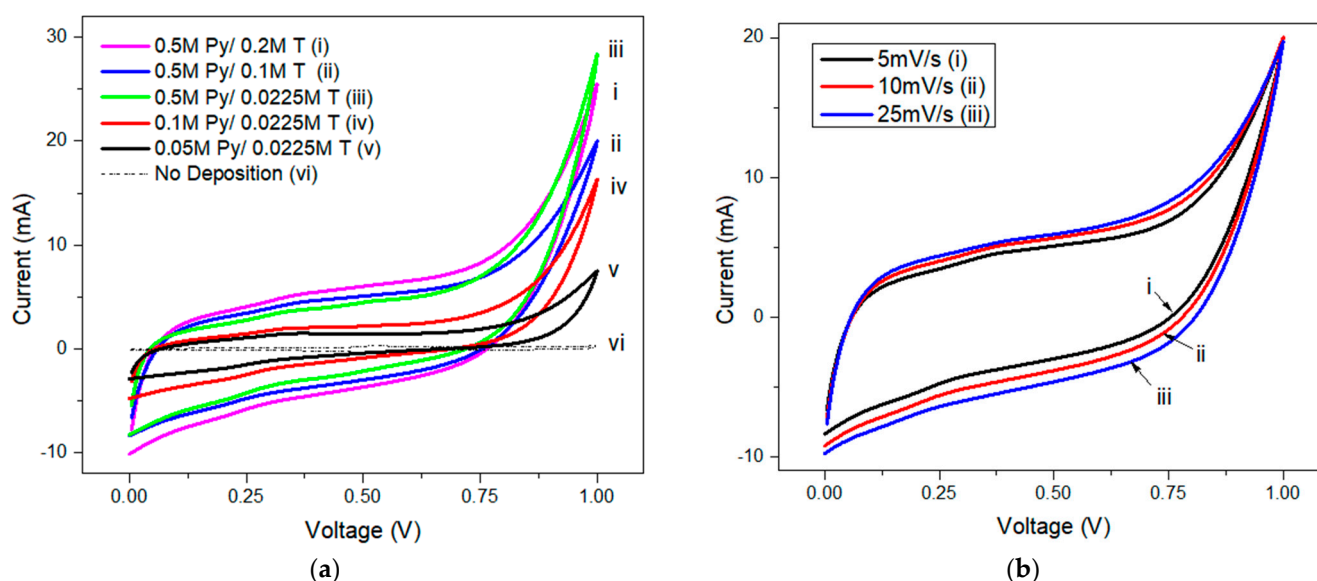


Figure 4. (a) 5 mV/s cyclic voltammograms of 50 wt%SWCNT/PI nanocomposite electrode with doped PPy at varying deposition conditions. (b) CV profile of nanocomposite electrode with electrodeposited PPy from a 0.5M Py/0.1M pTSA solution run at 5, 10, and 25 mV/s scan rates using a Ag/AgCl reference electrode.

Figure 5 highlights the trend in specific capacitance for the electrodes prepared at various deposition conditions and carried out at different scan rates. The highest specific capacitance obtained for the modified electrodes was 84.88 F/g at 5 mV/s for PPy formed from 0.5M Py/0.1M T solution. Increasing the dopant concentration to 0.2M reduced the C_p to 54.45 F/g, which is still higher than that for the same Py concentration but with a lower toluene sulphonic acid concentration of 0.0225M pTSA. A Lower Py concentration of 0.05 M showed a comparatively high C_p s of about 35 F/g. However, it was observed that the effect of increasing dopant concentration is a significant improvement in the electrode's specific capacitance due to the enhancement in the morphology of the electrode surface as shown by the optical micrographs. Electron migration due to delocalization of the conjugated bonds is enabled by doping, which lowers the energy barrier and improves conductivity as shown by the increase in current during te potentiostatic electrodeposition at 2 V in Figure 6 [33,34]. Figure 6 also shows that the steady-state transient current obtained during the electrochemical polymerization of pyrrole increases with increasing dopant concentration at a constant pyrrole concentration of 0.5M. Table 1 summarises the specific capacities obtained at the three different scan rates and calculated by using Equation (1b).

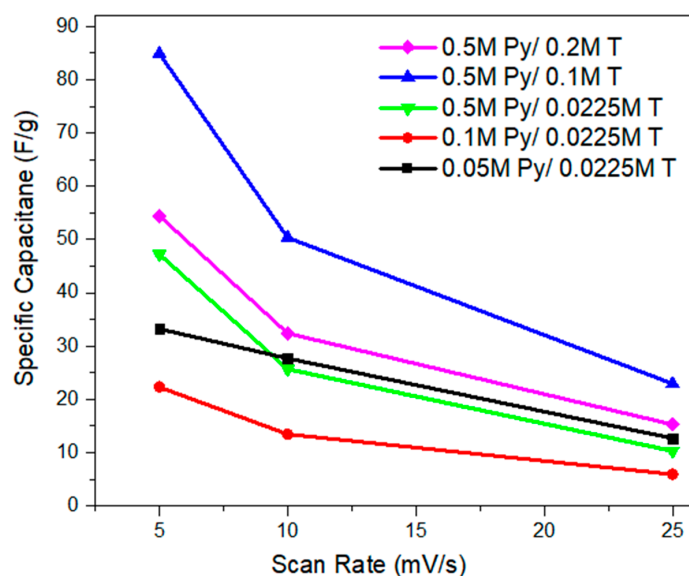


Figure 5. Summary of specific capacitance at each scan rate calculated from CV at 5, 10, and 25 mV/s.

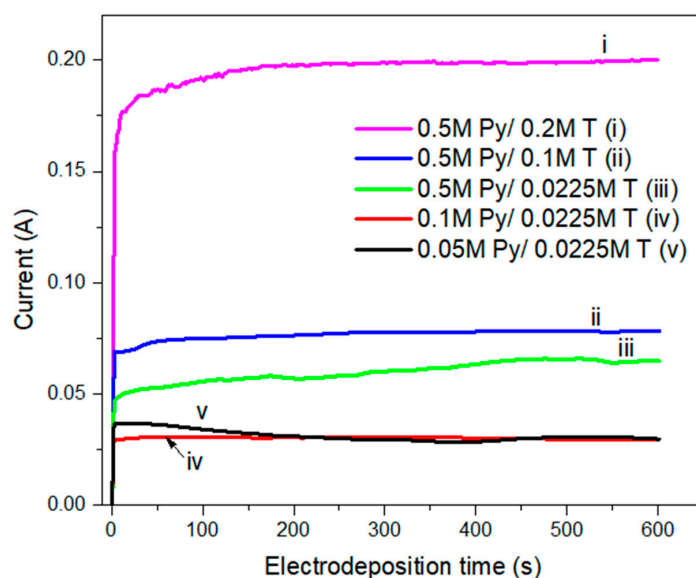


Figure 6. Transient current–time curves obtained during potentiostatic electrochemical polymerization of pyrrole onto the composite PI/SWCNT electrode.

Table 1. Calculated specific capacities using cyclic voltammetry.

600 s Deposition on 50 wt% SWCNT/PI Electrodes	Specific Capacity (mAh/g)		
	5 mV/s	10 mV/s	25 mV/s
0.05M Py/0.0225M T	9.230	7.702	3.529
0.1M Py/0.0225M T	6.194	3.735	1.652
0.5M Py/0.0225M T	13.116	7.132	2.861
0.5M Py/0.1M T	23.577	13.991	6.375
0.5M Py/0.2M T	15.124	9.000	4.243

4.3. Galvanostatic Charge/Discharge

The composite electrodes were subjected to 500 galvanostatic charge–discharge (GCD) cycles at current densities of 5 A/g, 1 A/g, and 0.5 A/g, respectively, using 1M H₂SO₄ electrolyte, in a voltage range between 0 and 0.8 V (Figure 7). A maximum discharge time of 200 s was obtained for 0.5M Py/0.1M T (Figure 7b) at a discharge current density of

0.5 A/g compared to 12.67 s for the system with 0.1M Py/0.0225M T (Figure 7a). The GCD profile of the electrode prepared by electrodepositing PPy from a 0.5M Py/0.1M T solution was relatively symmetrical with a negligible IR drop, showing that it experiences the electric double layer effect, which is associated with supercapacitor behavior [35].

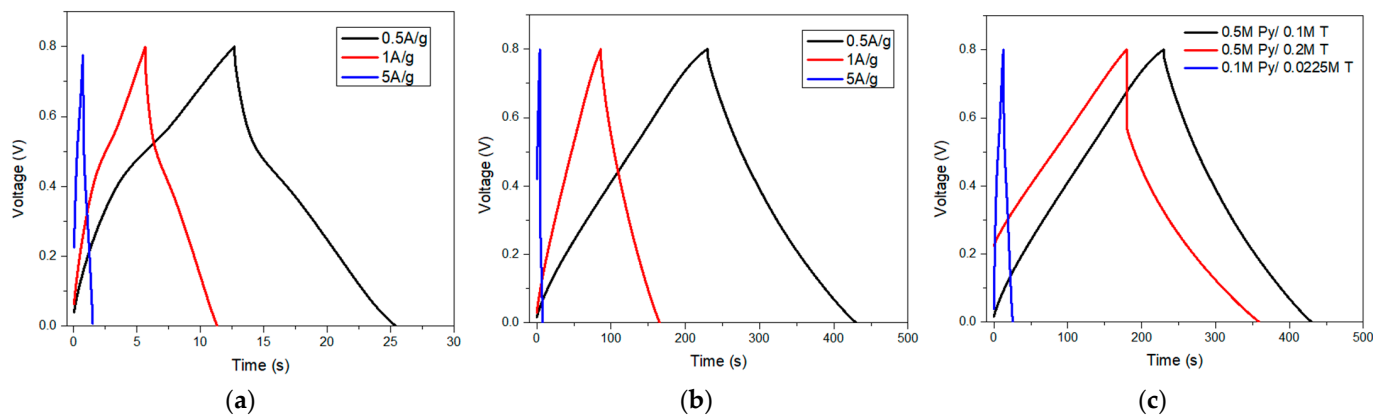


Figure 7. GCD curves for electrodes coated with PPy from (a) 0.1M Py/0.0225M T and (b) 0.5M Py/0.1M T at current densities of 0.5, 1, and 5 A/g. (c) GCD curves at 0.5 A/g for composite electrodes electro-coated with PPy from 0.5M Py/0.1M T, 0.5M Py/0.2M T, and 0.1M Py/0.0225M T solution, respectively.

Specific capacitance values as high as 127.13 F/g were obtained from the charge–discharge curves of composite electrodes coated with PPy from a solution containing 0.5M Py/0.1M T at 0.5 A/g, and as low as 7.89 F/g for composite electrodes electrodeposited with PPy from 0.1M Py/0.0225M T solution (Figure 8). Electrochemical deposition of PPy from higher pyrrole and dopant concentrations resulted in a significant improvement in the electrochemical performance of the electrodes. Table 2 summarizes the specific capacitance values, which were calculated using Equation (2).

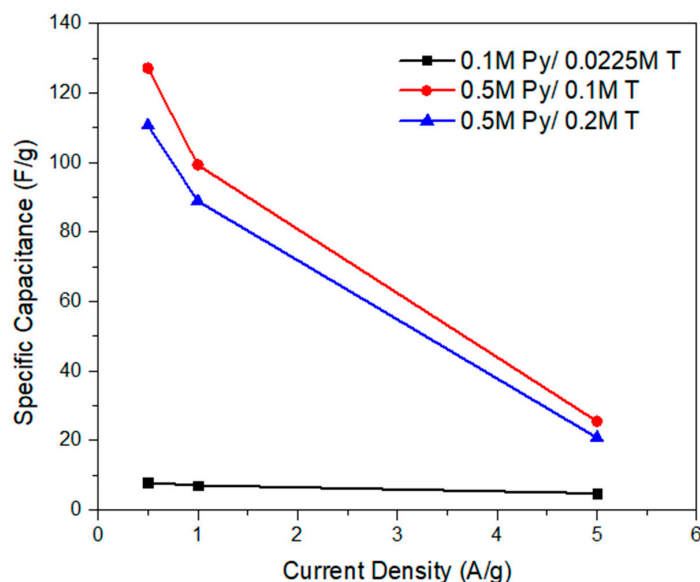


Figure 8. Specific capacitance of composite electrodes electrodeposited with PPy measured by using GCD at 0.5 A/g, 1 A/g, and 5 A/g.

The composite electrodes containing electrodeposited doped PPy showed relatively good cyclability with capacitance retention of over 80% through 500 cycles, as shown in Figure 9. The PPy electrodeposited from 0.5M Py/0.1M T solution maintained a capacitance retention of over 100% and was observed to increase its retention up to 120% at longer

cycles. Electrodes formed from lower concentrations of Py seem to show lower retention over the same duration.

Table 2. Summary of specific capacitance obtained from charge–discharge cycles at 0.5, 1, and 5 A/g.

600 s Deposition on 50 wt% SWCNT/PI Electrodes	Specific Capacitance (F/g)		
	0.5 A/g	1 A/g	5 A/g
0.1M Py/0.0225M T	7.89	7.12	4.82
0.5M Py/0.1M T	127.13	99.29	25.52
0.5M Py/0.2M T	110.65	88.88	20.79

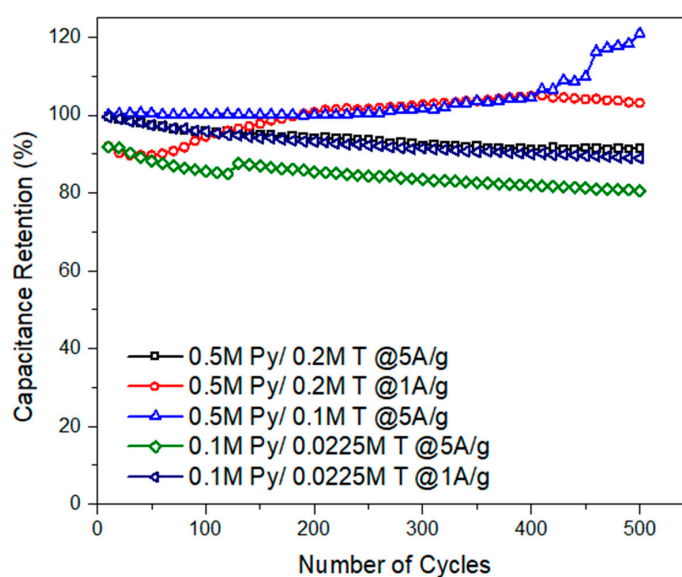


Figure 9. Capacitance retention for electrodes tested for over 500 cycles at current densities of 1 A/g and 5 A/g.

4.4. Electrochemical Impedance Spectroscopy (EIS)

EIS is a useful tool to analyze the mass transport of electrolytes through an electrode material. The material's porosity impacts this mass transport process as it creates different diffusion pathways through the channels and pores, affecting the electrochemical behavior of the material [30–32]. In this study, EIS measurements were carried out at a frequency range of 1 MHz to 0.01 Hz at 1 V open circuit potential.

A modified Randle's cell with a Warburg element equivalent electrical circuit was used to fit the data to obtain the bulk resistance of the electrodes, given the electrically conductive nature of the polymer [36]. The complex Nyquist plots are shown in Figure 10. The plots are very similar to those for traditional systems, with electrolyte diffusion occurring through their bulk. Lower resistance and capacitance occur at high frequencies due to the lack of electrolyte interaction within the material, although more so with its surface [3,37,38]. The Warburg impedance at lower frequencies shows the occurrence of diffusion through a porous network in the electrode [3].

As the Py concentration is increased, the bulk resistance decreases as the sample becomes more conductive and more porous. The bulk resistance, calculated using the equivalent electrical circuit model, is used to determine the theoretical porosity by using the modified form of Archie's law (Equations (3a) and (3b)). These values are presented in Table 3. It is shown that porosity is improved by the increasing Py concentration as well as by a complimentary increase in dopant concentration. The data for higher porosity electrodes agree with the C_p values calculated using CV and GCD, which shows that electrodes with higher porosity have improved electrochemical performances.

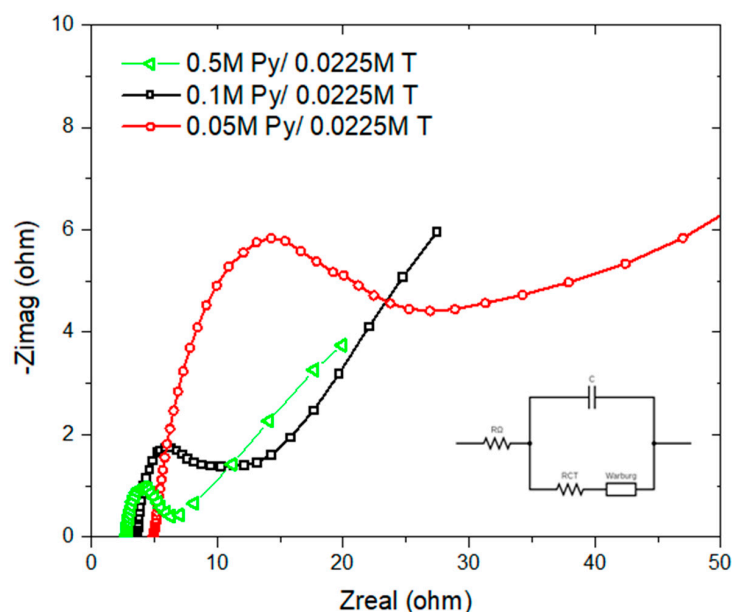


Figure 10. EIS: Nyquist plots showing the effect of Py concentration on electrodes with fixed dopant, modeled using equivalent Randle's cell circuit with Warburg element.

Table 3. Theoretical porosity and C_p obtained using EIS with a modified version of Archie's law.

600 s Deposition on 50 wt% SWCNT/PI Electrodes	Bulk Resistance (Ω)	Theoretical Porosity (%)	Specific Capacitance (F/g) Using EIS
0.05M Py/0.0225M T	57.04	5.67	7.07
0.1M Py/0.0225M T	13.70	14.66	15.37
0.5M Py/0.0225M T	5.47	27.05	40.52
0.5M Py/0.1M T	3.77	34.68	32.10
0.5M Py/0.2M T	2.55	44.94	15.06

The specific capacitance values were obtained towards the lower frequency end of the EIS spectrum using the modified equivalent electrical circuit model and Equation (4). Figure 10 and Table 3 show that the bulk resistance and specific capacitance of composite electrodes modified by the electrochemical deposition of PPy increased with increasing Py concentration at a constant dopant concentration. Increasing the pyrrole concentrations from 0.05M to 0.5M resulted in a corresponding increase in specific capacitance from 7 F/g to 40.5 F/g at a constant dopant concentration of 0.0225M. The trend of the EIS data is similar to the results from the other electrochemical techniques, although with lower C_p values. Increasing the dopant concentrations from 0.0225M to 0.2M does not seem to result in increased specific capacitance.

4.5. Fourier Transform Infrared Spectroscopy—FTIR

Figure 11 shows a broad peak in the 3522 cm^{-1} region, which could be attributed to N-H stretching; peaks around 1170 cm^{-1} indicate the N-C stretch bending, and a sharp but shallow peak around 1558 cm^{-1} comes from the C=C. A peak of about 1300 cm^{-1} comes from the C-N stretching. The sharp peak around 800 cm^{-1} comes from the aromatic C-H bending. These peaks as summarized in Table 4 confirm that PPy has indeed been formed on the electrode material. Peaks around 1700 cm^{-1} indicate the characteristic imide bands that belong to the polyimide substrate.

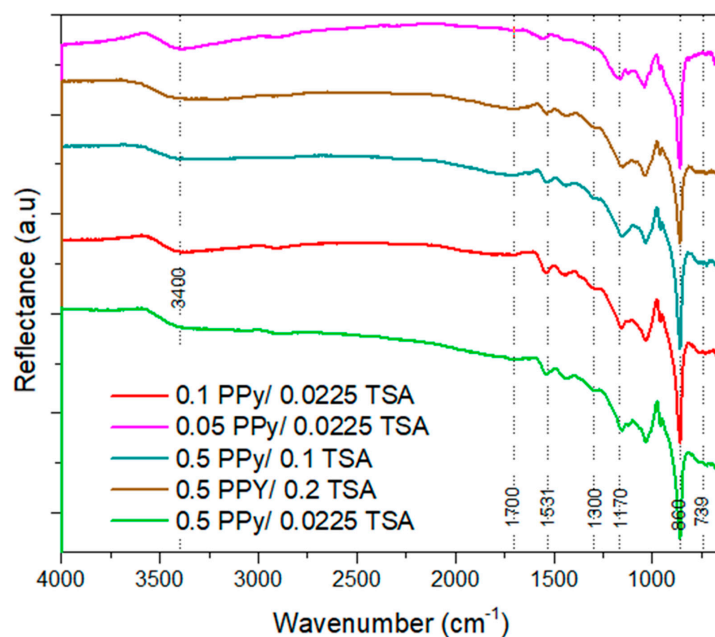


Figure 11. FTIR spectra of PPy doped with pTSA.

Table 4. Characteristic FTIR peaks and corresponding functional groups.

Characteristic Wavenumber (cm ⁻¹)	Functional Group
3500–3300	N-H amine stretch
1700	C=C aromatic bending
1561–1531	C=C/C-C stretching
1300	C-N stretching
1170	N-C stretch bending
860	C-H bending
739	C=O bending

5. Conclusions

A single-walled carbon nanotube/polyimide nanocomposite electrode was synthesized and modified by the electrodeposition of p-Toluene sulfonic acid-doped polypyrrole. The deposition from higher concentrations of Py was observed to have changed the morphology of the nanocomposite surface by improving its porosity. The electrochemical performance of the electrodes was further enhanced by the increase in dopant concentration. Cyclic voltammetry and galvanic charge–discharge tests were carried out, and maximum specific capacitances of 84.88 F/g and 127.13 F/g, respectively, were obtained for the electrodeposition of doped PPy from a solution containing 0.5M Py and 0.1M pTSA. At a max of 0.2M TSA, it was noticed that there was increased flaking off of the doped PPy deposition on the electrode as well as reduced performance in the system. A capacitance retention of greater than 80% was also obtained after 500 cycles of testing with the composite electrode formed from 0.5M Py/0.1M T solution, which showed an improved capacitance retention with increasing cycles. At higher Py concentrations, a thicker layer of PPy was deposited on the surface of the electrode. As the electrode undergoes longer charge discharge cycles, this also allows for more time for the electrolyte to have saturated through the bulk of the electrode. As a result, more surface area for electrolyte/electrode interaction is presented, in turn increasing the covered surface area to more than 100%. Galvanic charge–discharge tests also showed almost symmetrical charging and discharging trends, indicating the material's supercapacitor-like properties, with broad potential uses in the energy storage sector.

Author Contributions: Conceptualization, J.O.I. and R.G.; methodology, J.O.I. and R.G.; software, R.G.; validation, J.O.I. and R.G.; formal analysis, R.G.; investigation, R.G.; resources, J.O.I.; data curation, R.G.; writing—original draft preparation, R.G.; writing—review and editing, J.O.I. and R.G.; visualization, J.O.I.; supervision, J.O.I.; project administration, J.O.I.; funding acquisition, J.O.I.; All authors have read and agreed to the published version of the manuscript.

Funding: This research received no external funding.

Data Availability Statement: Not applicable.

Acknowledgments: The support provided by the Mechanical and Materials Engineering Department and the Sensors laboratory in the Chemistry Department at the University of Cincinnati, is hereby acknowledged.

Conflicts of Interest: The authors declare no conflict of interest.

References

1. Conway, B.E. *Electrochemical Supercapacitors: Scientific Fundamentals and Technological Applications*; Plenum Press: New York, NY, USA, 1999.
2. Ellenbogen, J.C. *Supercapacitors: A Brief Overview*; The MITRE Corporation: McLean, VA, USA, 2006.
3. Okafor, P.A.; Huxel, B.; Iroh, J.O. Electrochemical behavior of multifunctional graphene-polyimide nanocomposite film in two different electrolyte solutions. *J. Appl. Polym. Sci.* **2015**, *132*, 1–9. [[CrossRef](#)]
4. Ansaldo, A.; Bondavalli, P.; Bellani, S.; Castillo, A.E.D.R.; Prato, M.; Pellegrini, V.; Pognon, G.; Bonaccorso, F. High-power graphene–Carbon nanotube hybrid supercapacitors. *ChemNanoMat* **2017**, *3*, 436–446. [[CrossRef](#)]
5. Wang, F.; Wu, X.; Yuan, X.; Liu, Z.; Zhang, Y.; Fu, L.; Zhu, Y.; Zhou, Q.; Wu, Y.; Huang, W. Latest advances in supercapacitors: From new electrode materials to novel device designs. *Chem. Soc. Rev.* **2017**, *46*, 6816–6854. [[CrossRef](#)] [[PubMed](#)]
6. Khomenko, V.; Frackowiak, E.; Béguin, F. Determination of the specific capacitance of conducting polymer/nanotubes composite electrodes using different cell configurations. *Electrochim. Acta* **2005**, *50*, 2499–2506. [[CrossRef](#)]
7. Molina, J.; Esteves, M.F.; Fernández, J.; Bonastre, J.; Cases, F. Polyaniline coated conducting fabrics. Chemical and electrochemical characterization. *Eur. Polym. J.* **2011**, *47*, 2003–2015. [[CrossRef](#)]
8. Uyar, T.; Toppare, L.; Hacaloğlu, J. Characterization of electrochemically synthesized p-toluene sulfonic acid doped polypyrrole by direct insertion probe pyrolysis mass spectrometry. *J. Anal. Appl. Pyrolysis* **2002**, *64*, 1–13. [[CrossRef](#)]
9. Campomanes, R.; Bittencourt, E.; Campos, J.S.C. Study of conductivity of polypyrrol-poly(vinyl alcohol) composites obtained photochemically. *Synth. Met.* **1999**, *102*, 1230–1231. [[CrossRef](#)]
10. Wallace, G.G.; Spinks, G.M.; Leon, P.; Teasdale, P.R. *Conductive Electroactive Intelligent Materials Systems*; CRC Press: New York, NY, USA, 2003.
11. Rahaman, M.; Aldalbahi, A.; Almoqli, M.; Alzahly, S. Chemical and electrochemical synthesis of polypyrrole using carrageenan as a dopant: Polypyrrole/multi-walled carbon nanotube nanocomposites. *Polymers* **2018**, *10*, 632. [[CrossRef](#)]
12. Jaworska, E.; Michalska, A.; Maksymiuk, K. Polypyrrole Nanospheres–Electrochemical Properties and Application as a Solid Contact in Ion-selective Electrodes. *Electroanalysis* **2017**, *29*, 123–130. [[CrossRef](#)]
13. Bashid, H.A.A.; Lim, H.N.; Kamaruzaman, S.; Rashid, S.A.; Yunus, R.; Huang, N.M.; Yin, C.Y.; Rahman, M.M.; Altarawneh, M.; Jiang, Z.T.; et al. Electrodeposition of Polypyrrole and Reduced Graphene Oxide onto Carbon Bundle Fibre as Electrode for Supercapacitor. *Nanoscale Res. Lett.* **2017**, *12*, 1–10.
14. Parayangattil Jyothibas, J.; Chen, M.Z.; Lee, R.H. Polypyrrole/Carbon Nanotube Freestanding Electrode with Excellent Electrochemical Properties for High-Performance All-Solid-State Supercapacitors. *ACS Omega* **2020**, *5*, 6441–6451. [[CrossRef](#)] [[PubMed](#)]
15. Levine, K.; Iroh, J.O. Electrochemical behavior of a composite of polyimide and polypyrrole. *J. Mater. Chem.* **2001**, *11*, 2249–2253. [[CrossRef](#)]
16. Ramanavičius, A.; Ramanavičiene, A.; Malinauskas, A. Electrochemical sensors based on conducting polymer-polypyrrole. *Electrochim. Acta* **2006**, *51*, 6025–6037. [[CrossRef](#)]
17. Lee, J.Y.; Kim, D.Y.; Kim, C.Y. Synthesis of soluble polypyrrole of the doped state in organic solvents. *Synth. Met.* **1995**, *74*, 103–106. [[CrossRef](#)]
18. Shen, Y.; Wan, M. In situ doping polymerization of pyrrole with sulfonic acid as a dopant. *Synth. Met.* **1998**, *96*, 127–132. [[CrossRef](#)]
19. Lü, Q. Unstirred preparation of soluble electroconductive polypyrrole nanoparticles. *Microchim. Acta* **2010**, *168*, 205–213. [[CrossRef](#)]
20. Dong, Z.H.; Wei, Y.L.; Shi, W.; Zhang, G.A. Characterisation of doped polypyrrole/manganese oxide nanocomposite for supercapacitor electrodes. *Mater. Chem. Phys.* **2011**, *131*, 529–534. [[CrossRef](#)]
21. DiLeo, R.A.; Frisco, S.; Ganter, M.J.; Rogers, R.E.; Raffaele, R.P.; Landi, B.J. Hybrid germanium nanoparticle-single-wall carbon nanotube free-standing anodes for lithium ion batteries. *J. Phys. Chem. C* **2011**, *115*, 22609–22614. [[CrossRef](#)]

22. Bandaru, P.R. Electrical properties and applications of carbon nanotube structures. *J. Nanosci. Nanotechnol.* **2007**, *7*, 1239–1267. [[CrossRef](#)]
23. So, H.H.; Cho, J.W.; Sahoo, N.G. Effect of carbon nanotubes on mechanical and electrical properties of polyimide/carbon nanotubes nanocomposites. *Eur. Polym. J.* **2007**, *43*, 3750–3756. [[CrossRef](#)]
24. Iroh, J.; Levine, K.; Shah, K.; Zhu, Y.; Donley, M.; Mantz, R.; Johnson, J.; Voevodin, N.; Balbyshev, V.; Khramov, A. Electrochemical behaviour of conducting polymer/polyimide composite. *Surf. Eng.* **2004**, *20*, 93–98. [[CrossRef](#)]
25. Seetala, N.; Hendon, C.; Tull-Walker, N.; Van Behr, J.; Hester, B.; Lebron-Colon, M.; Meador, M. Synthesis and characterization of polyimide-carbon nanotube composites. *World J. Eng.* **2014**, *11*, 193–198. [[CrossRef](#)]
26. Kareem, A.A. Preparation and electrical properties of polyimide/carbon nanotubes composites. *Mater. Sci. Pol.* **2017**, *35*, 755–759. [[CrossRef](#)]
27. Xiao, S.; Akinyi, C.; Longun, J.; Iroh, J.O. Polyimide Copolymers and Nanocomposites: A Review of the Synergistic Effects of the Constituents on the Fire-Retardancy Behavior. *Energies* **2022**, *15*, 4014. [[CrossRef](#)]
28. Huang, G.; Zhang, Y.; Wang, L.; Sheng, P.; Peng, H. Fiber-based MnO₂/carbon nanotube/polyimide asymmetric supercapacitor. *Carbon N. Y.* **2017**, *125*, 595–604. [[CrossRef](#)]
29. Wang, H.; Yi, H.; Chen, X.; Wang, X. Asymmetric supercapacitors based on nano-architected nickel oxide/graphene foam and hierarchical porous nitrogen-doped carbon nanotubes with ultrahigh-rate performance. *J. Mater. Chem. A* **2014**, *2*, 3223–3230. [[CrossRef](#)]
30. Neithalath, N.; Weiss, J.; Olek, J. Characterizing Enhanced Porosity Concrete using electrical impedance to predict acoustic and hydraulic performance. *Cem. Concr. Res.* **2006**, *36*, 2074–2085. [[CrossRef](#)]
31. Tully-Dartez, S.; Cardenas, H.E.; Sit, P.F.S. Pore characteristics of chitosan scaffolds studied by electrochemical impedance spectroscopy. *Tissue Eng.-Part C Methods* **2010**, *16*, 339–345. [[CrossRef](#)]
32. Shi, K.; Ren, M.; Zhitomirsky, I. Activated carbon-coated carbon nanotubes for energy storage in supercapacitors and capacitive water purification. *ACS Sustain. Chem. Eng.* **2014**, *2*, 1289–1298. [[CrossRef](#)]
33. Tian, F.; Zhang, Y.; Liu, L.; Zhang, Y.; Shi, Q.; Zhao, Q.; Cheng, Y.; Zhou, C.; Yang, S.; Song, X. Spongy p-Toluenesulfonic Acid-doped Polypyrrole with Extraordinary Rate Performance as Durable Anodes of Sodium-Ion Batteries at Different Temperatures. *Langmuir* **2020**, *36*, 15075–15081. [[CrossRef](#)]
34. Andleeb, S.; Kumar Singh, A.; Eom, J. Chemical doping of MoS₂ multilayer by p-toluene sulfonic acid. *Sci. Technol. Adv. Mater.* **2015**, *16*, 35009. [[CrossRef](#)] [[PubMed](#)]
35. Moysowicz, A.; Gryglewicz, G. High-performance hybrid capacitor based on a porous polypyrrole/reduced graphene oxide composite and a redox-active electrolyte. *Electrochim. Acta* **2020**, *354*, 136661. [[CrossRef](#)]
36. Shukla, A.; Sen, K.; Das, D. Studies on electrolytic and doping behavior of different compounds and their combination on the electrical resistance of polypyrrole film via electrochemical polymerization. *J. Appl. Polym. Sci.* **2022**, *139*. [[CrossRef](#)]
37. Zhu, Y.; Iroh, J.O.; Rajagopalan, R.; Aykanat, A.; Vaia, R. Optimizing the Synthesis and Thermal Properties of Conducting Polymer–Montmorillonite Clay Nanocomposites. *Energies* **2022**, *15*, 1291. [[CrossRef](#)]
38. Zhu, Y.; Kottarath, S.; Iroh, J.O.; Vaia, R.A. Progressive Intercalation and Exfoliation of Clay in Polyaniline–Montmorillonite Clay Nanocomposites and Implication to Nanocomposite Impedance. *Energies* **2022**, *15*, 5366. [[CrossRef](#)]